Journal of Cluster Science, Vol. 13, No. 4, December 2002 (© 2002)

Preparation of Phase Pure Cubic Gallium Nitride, *c*-GaN, by Ammonothermal Conversion of Gallium Imide, $\{Ga(NH)_{3/2}\}_n$

R. Jason Jouet,[1] Andrew P. Purdy,[2,5] Richard L. Wells,[3] and Jerzy F. Janik[4]

Received May 16, 2002

Gallium imide, $\{Ga(NH)_{3/2}\}_n$, was sealed in quartz tubes with anhydrous NH_3 and NH_4X (X = Cl, Br, I) and heated vertically in an autoclave with the hot-zone (bottom) temperature ranging from 300–530 °C. With NH_4I mineralizer, the imide was converted to primarily the zinc-blende phase of GaN (*c*-GaN), usually in the form of micron sized or smaller tetrahedra. With NH_4Cl mineralizer, hexagonal GaN nanoparticles formed instead, and NH_4Br facilitated the conversion of imide to irregular *h*-GaN nanoparticles at lower temperatures, and larger particles above 500 °C. At the higher temperatures, chemical transport took place and GaN crystals grew on the walls at the middle to the top of the tube. Most of the deposited GaN was cubic, usually in a heavily etched triangular prismatic morphology. Several experiments were performed in a Pt lined pressure vessel in order to demonstrate that the synthesis method can be scaled up.

KEY WORDS: Zinc-blende; gallium nitride; nanoparticles; crystal growth; synthesis.

INTRODUCTION

The recent development and commercialization of blue-light emitters, blue diode lasers, and optical communications based on gallium nitride has

[1] Indian Head Division, Naval Surface Warfare Center, Research and Technology Department, 101 Strauss Ave., Indian Head, Maryland 20640.

[2] Naval Research Laboratory, Chemistry Division, Code 6125, Washington, District of Columbia 20375-5342.

[3] Retired. Current address: N8753 1010th Street, River Falls, Wisconsin 54022.

[4] Faculty of Fuels and Energy, University of Mining and Metallurgy, Krakow, Poland.

[5] To whom correspondence should be addressed. E-mail: purdy1@ccs.nrl.navy.mil PH 202-404-7444

1040-7278/02/1200-0469/0 © 2002 Plenum Publishing Corporation

propelled the material into the spotlight of interest. There are many advantages of using GaN films, namely, high chemical inertness, radiation resistance, and the capability of working at elevated temperatures with high quantum efficiency. GaN is also ideal for high power applications because of its large avalanche breakdown field, high thermal conductivity, and large high field electron drift velocity [1, 2].

There are, however, many obstacles to the growth of epitaxial device quality GaN films with low defect densities and dopant concentrations. Among the most significant of these are the lack of suitably lattice-matched substrates and the divergent thermal expansion coefficients of the typical sapphire or SiC substrate and gallium nitride. The disparate coefficients of thermal expansion between substrate and material induce residual stresses in the film upon cooling. Currently, the production of thin films of GaN is carried out by MOCVD heteroepitaxy from $Ga(CH_3)_3$ or $Ga(C_2H_5)_3$ and ammonia on sapphire (Al_2O_3) substrates. However, due to the aforementioned divergent thermal expansion coefficients between gallium nitride and the substrate materials, the nitride films have a large number of defects. Therefore, the best substrate for low defect GaN films should be suitably sized single crystals of GaN [3].

Gallium nitride has at least three distinct crystalline morphologies—the common hexagonal wurtzite structure, the metastable cubic zinc blende structure and a high pressure rocksalt structure. Compared to hexagonal (wurtzite) GaN, however, the metastable cubic (zinc blende) phase of GaN has several potential advantages for device application including easy cleavage, smaller bandgap, and higher carrier mobilities [4]. It was also recently shown that the ionization energy of shallow acceptors in cubic GaN (*c*-GaN) is slightly less than that observed in hexagonal GaN (*h*-GaN). This property of *c*-GaN results in an increased hole concentration in p-type layers and in consequence the potential for more efficient light emitting devices. Finally, zinc blende GaN might be more readily integrated with existing high quality III-V semiconductor substrates and devices as most of the III-V semiconductors adopt the cubic form [3].

Single crystals of hexagonal wurtzite GaN have been prepared by high-pressure vapor transport [5], solution growth from a metallic flux [6–9], ammonothermal methods using alkaline mineralizers [10–12], and chemical vapor transport processes [13, 14], among others. Zinc-blende phase GaN single crystals, however, have been more difficult to obtain. Thin films of *c*-GaN have been grown only by chemical vapor deposition on nearly lattice-matched substrates such as gallium arsenide [1–3], and single crystals have been grown only in potassium metal flux [9] and by ammonothermal techniques.

Recently, Purdy [15] reported the preparation of bulk crystalline *c*-GaN in an acidic supercritical NH_3 medium at temperatures as low as 275°C. Deposits of *c*-GaN crystals were prepared from Ga metal and NH_3/NH_4X (X = Cl, Br, I), from ammonolysis of GaI_3, and from acidic ammonolysis of cyclotrigallazane [16]. However at up to 30 μm in length, these crystals were not large enough to be used as substrates for device applications. In addition, the reaction of gallium metal with NH_3/NH_4X forms dihydrogen and consumes NH_3, which results in changing conditions during the reaction and thus makes the process scale dependent. When GaI_3 was used as a starting material, the formation of GaN was accompanied by the production of large quantities of NH_4I, which limits the concentration, but not the scale at which the reaction can be performed. Ga imide-iodide materials were also used as a Ga source, but the compositions of the imide-iodides were difficult to reproduce and depended on the presence of silicone contamination in order to produce crystalline *c*-GaN.

In attempt to eliminate the problems of NH_3 consumption, excess dihydrogen or NH_4I production during ammonothermal GaN formation, or the need to synthesize hard to reproduce starting materials, we investigated the use of pure *h*-GaN and the use of the pure gallium imide compound, $\{Ga(NH)_{3/2}\}_n$ (**1**) [17], as the Ga source. An account of *h*-GaN as a feedstock for *c*-GaN crystal growth was published elsewhere [18]. The production of **1** by ammonolysis of $Ga(NMe_2)_3$ is highly reproducible and avoids the problems associated with reactions between GaI_3 and KNH_2. In this work, both small scale ammonothermal conversion of **1** to *c*-GaN in sealed quartz tubes and a few preliminary experiments at larger scale conversion in a platinum lined pressure vessel were accomplished with the use of an ammonium halide mineralizer, NH_4X (X = Cl, Br, I).

EXPERIMENTAL

Gallium imide, $\{Ga(NH)_{3/2}\}_n$, (**1**) was prepared according to previously reported methods using appropriate Schlenk line procedures [17]. Most experiments used pure **1**, but a siloxane contaminated imide was used in a few reactions (see below). $HNMe_2$ and n-BuLi (2.5 M solution in hexanes) were purchased from Aldrich and used as received. NH_4X (X = Cl, Br, I) was purchased from Aldrich and sublimed prior to use. LiX (X = Cl, Br, I) was also purchased from Aldrich and was dried by heating under vacuum. All solid reactants were handled in a Vacuum Atmospheres Dri Lab under a He atmosphere.

Siloxane Contaminated Imide. During the preparation of one of the batches of gallium imide, a small amount of silicon oil sucked back from a

bubbler into the reaction between n-BuLi and $HNMe_2$ prior to addition to the $GaCl_3$. Some products from siloxane cleavage, presumably compounds of the form $Ga(NMe_2)_2(OSiMe_2)_nSiMe_3$, were still visible in the ^1H NMR spectrum of the $Ga(NMe_2)_3$ after sublimation, and the gallium imide prepared from this material is designated **1a**, and was used in a few ammonothermal experiments.

Sealed Tube Experiments

Anhydrous ammonia was condensed (at −196°C) into 7 in.-long, 5 mm OD, 3-mm ID quartz tubes containing the reactants. The tube was flame-sealed at a height (interior measure) of about 13–17 cm. The exterior of the tube was pressurized with water inside an MRA-114R pressure vessel attached to a Leco HR-1B hydrothermal system to 10,000 psi. The pressure vessel was then heated in a vertical orientation. All reaction temperatures were measured in the thermowell near the bottom of the pressure vessel (hot zone). The temperature gradients going up the tube were substantial, on the order of −10°C/cm [15]. After completion of the temperature program, the tubes were allowed to cool at a natural rate (up to 2 h) to less than 200°C before lowering the furnace, and to room temperature before removal from the pressure vessel. All tubes were frozen at −196°C before opening, and the products were washed with copious amounts of 1 M HCl, H_2O, EtOH and Acetone, and air-dried. A listing of experiments is provided in Table I. The mass fraction of each GaN product in the hexagonal and cubic phases was determined by comparison of its x-ray powder pattern to that of a well-ground 50:50 mixture of *h*-GaN and *c*-GaN.

Large Scale Experiments

For exp #82: While working in a dry box under continuous N_2 purge, **1** (4.1 g; 44.4 mmol based on Ga) and NH_4I (3.06 g; 21.1 mmol) was loaded into an Al_2O_3 crucible which had been heated in a 200°C oven. This was cooled in liquid N_2 and placed into a N_2 cooled Leco LRA-150RB pressure vessel with a Pt liner (O. D. 3 in.; I. D. 1.5 in.; internal volume 175 ml). NH_3 was poured into the vessel to a level approximately 1.5 in. below the top of the liner. A Pt disk was then placed over the mouth and the vessel was sealed. The vessel was then heated in the vertical orientation behind a blast shield to 485°C for a period of 14 days. The vessel was then allowed to cool to room temperature and further cooled with liquid N_2 prior to opening. After the NH_3 was vented, the loose gray deposit band on the vessel wall, about 1–3″ below the top, was carefully scraped out (#2, 36 mg), and the crucible was removed and its contents washed in

the same manner as the material from the sealed tube reactions, affording 785 mg of a yellow powder (#1). About 83 mg of materials that were mixtures of #1 and #2 were also isolated. The other experiments were done in a similar manner (Table I)

DISCUSSION

Sealed Tube Experiments

All products of the ammonothermal reactions (Table I) were examined by x-ray powder diffraction and by SEM, and data from selected experiments can be found in Figs. 1 and 2, respectively. It is evident from the x-ray diffraction data that the mineralizer used is necessary for the low temperature conversion of **1** to GaN, as the experiment without mineralizer (#78) produced a nanocrystalline, almost amorphous product at 463°C. There also seems to be an important and decisive correlation between the halide ion and both the phase of the final material as well as the transport of the crystals in the tube. From these experiments it seems that NH_4I is the most effective mineralizer for the conversion of **1** to *c*-GaN and the transport and crystal growth of the latter. As with prior work, little or no material is transported to the upper portions of the tubes at the lower temperatures, and at the highest temperatures most or all of the GaN transports. The material produced at the bottom of the tube (hot zone) in reactions containing NH_4I was yellow to orange and the material that deposited in the middle or top of the tubes (cool zone) was orange to bright orange. Nearly all of the GaN formed from ammonothermal conversion of **1** using NH_4I as the mineralizer was cubic. The deposits were 100% cubic in every case where the tube was heated rapidly to its final temperature, but the two experiments (#67 and 69) that involved a stepwise heating profile had some *h*-GaN in the deposit. The powders at the bottom of the tube were entirely *c*-GaN except the ones made at 479 and 506°C (exp #72 and 70).

A few experiments were conducted with an imide batch **1a** where the $Ga(NMe_2)_3$ synthesis became contaminated with silicone oil from a bubbler prior to its conversion to imide. The presence of these impurities was highly detrimental for conversion of **1a** to *c*-GaN in exp #79 and 80. When NH_4I mineralizer was used, the powders produced at the tube bottoms were amorphous or had broad peaks in the x-ray powder pattern. Mechanical blockages also tended to form in the middle of the tubes, and at the higher temperature (exp #79) a large amount of gray *h*-GaN deposited near the mechanical blockage.

Table I. Experimental Data for Crystal Growth of GaN from $\{Ga(NH)_{3/2}\}_n$, (1) and Selected Mineralizer Agents

Exp #	Reactants mg, [mmol] $Ga(NH)_{3/2}$	NH_4X	NH_3	E. Temp. (16.7h)	Bottom of tube visual, xrd, SEM	mg	Middle of tube visual, xrd, SEM	mg	Top of tube vis, xrd, SEM	mg
63	108.1 [1.171]	**{I}** 103.3 [0.713]	[19.5] 8.8/14.4 cm fill	510	or pwdr 100% cub 1 µm ▲ + irr	6.0	thick brt or dep, cub 20 µm (l) ◬ + 15 µm plates	79.9	no dep.	N/A
64	102.8 [0.297]	**{Br}** 76.2 [0.778]	[19.5] 8.6/14.4 cm	509	yel-green pdr, 100% hex 1 µm ⊙	14.8	yel-grn-gray dep, 70% cub/30% hex, close to bottom of tube, 500 nm ⊳	48.2	yel-grn dep cub 5–15 µm irr ndl.	2.7
65	102.3 [1.109]	**{Cl}** 36.4 [0.681]	[19.5] 8/14.5 cm	511	pale green pwdr xrd-amorphous < 50 nm ⊙	52.9	no deposit	N/A	lt grn dep, hex irr ⊙	29.9
66	108.4* [1.175]	**{I}** 110.4 [0.762]	[19.5] 8.8/14.1 cm	302	lt-or pwdr > 95% cub 1 µm ▲ + irr	93.2	lt or. dep., cub < 1 mm ▲ + irr	6.0	no dep.	N/A
67	110* [1.192]	**{I}** 112 [0.773]	[19.5] 9.2/14.3 cm	305 (63.5h) 392 448	pale or pwdr, 100% cub 1 µm ▲ + irr	72.1	small or cluster dep. 92% cub/8% hex 6 × 30 µm ⊳	2.4	no dep.	N/A
68	125.4* [1.359]	**{I}** 123.8 [0.854]	[19.5] 9.1/14.2 cm	448 (64.3h)	or pwdr, 100% cub irr + 0.5–1 µm ▲	95.8	thick brt or dep, 100% cub 5 × 50 µm ⊳	37.3	lt or/yel dep 100% cub, < 10 µm ndl, ⅄ + < 1 µm ◆	3.4
69	58.0* [0.629]	**{I}** 53.0 [0.366]	[19.5] 8.8/14.1 cm	297 530	no material	N/A	or/yel/green 90% cub/10% hex 10 × 30 µm ◬, ✶, ⩓	31.5	or/yel dep, 100% cub ◬	16.3

70	155.0* [1.680]	**{I}** 161.0 [1.110]	[19.5] 9.3/14.2 cm	506 (21h)	or pwdr 90% cub/10% hex > 1 μm agglom. ▲ + irr ⊙	45.9	thick brt or dep, 100% cub 2 × 10 μm irr ndl	47.0	no dep	N/A
71	106.7 [1.157]	**{I}** 103.0 [0.711]	[25.0 11.2/17.1 cm	375	or pwdr, 100% cub 1 μm ▲	66.6	thin, faint yel/or dep 100% cub < 1 μm ▲ + irr	1.0	no dep	N/A
72	128.0 [1.387]	**{I}** 137.0 [0.945]	[25.0] 11.3/17 cm	479	yel/or pwdr 85% cub/15% hex 1 μm ▲ + 0.5 μm hex. prism	58.7	yel/or dep w/ clusters 100% cub 2 × 10 μm ⋗ + 250 nm ▲	22.0	no dep	N/A
73	110.0 [1.192]	**{I}** 135.0 [0.931] **LiI** 113.0 [0.844]	[25.0] 12.1/17.1 cm	459	gray/yel pwdr 50% cub/50% hex 300–500 nm ▲ + 200 nm hex prism	55.6	lt yel dep 100% cub 200–600 nm △ + irr	17.0	no dep	N/A
74	107.5 [1.165]	**{Br}** 77.0 [0.786]	[25.0] 11.3/16.7 cm	478	faint lt green pwdr 100% hex irr. nano ⊙	12.6	drk thick army green dep 100% cub 5–10 × 25 μm ◬	40.8	no dep	N/A
75	111.1 [1.204]	**{Br}** 77.3 [0.789] **LiBr** 78.2 [0.900]	[25.0] 11/16.9 cm	454	lime grn pwdr dissolved completely in H_2O discarded		lt lime green dep amorphous, w/ some cubic character 200–400 nm ▲	48.7	no dep	N/A
76	108.3 [1.174]	**{I}** 104.5 [0.721]	[25.0] 10.4/17 cm	521	no material	N/A	thick or dep 100 % cub ◬	87.8	no material	N/A
77	112.3 [1.22]	**{Cl}** 38.4 [0.72]	[25.0] 11.2/17.3 cm	465	lt grn pwdr irr 50 nm ⊙		lt grn dep 300 nm hex plate + △			
78	111.3 [1.21]	**none**	[19] 8.5/13.9 cm	463	off-wh/grn pwdr irr ∼ 25 nm ⊙		N/A			

Table I. *(Continued)*

Exp #	Reactants mg, [mmol] $Ga(NH)_{3/2}$	NH_4X	NH_3	E. Temp. (16.7h)	Bottom of tube visual, xrd, SEM	mg	Middle of tube visual, xrd, SEM	mg	Top of tube vis, xrd, SEM	mg
79	120 (**1a**) [1.30]	{**I**} 75 [0.52]	[25.0] 11.5/16.9 cm	505	yel pwdr, 65% cub irr agglomerate of < 50 nm ⊙	26.3	yel dep 90% cub 2 × 5 μm ◬	1.3		
							grey dep 95% 10–250 μm ‖	15.7		
							dk gr plug 60% 150 μm ‖ + 5 μm ⋗	7.2		
							loose yl pwdr, cub △ + irr, ⩽ 1 μm	8.3		
80	78 (**1a**) [0.85]	{**I**} 71 [0.49]	[14.6] 7.5/15.8 cm	417–437	brn pwdr, amor agglomerate of 50 nm–1 μm ⊙	18.4	yel dep, 98% cub < 10 μm clusters of △ and ◬	18.1		
					Large vessel					
81	630 [6.83]	{**I**} 610 [4.21]	~ 50% fill @ − 33 °C	~ 300, 400	yel pdr, cub 200–400 nm, 1 μm ▲ + irr	90	no transport			
82	4060 [44.0]	{**I**} 3060 [21.1]	~ 75% fill @ − 33 °C	487 °C, 14d	yel pdr, 90% cub 200–400 nm ▲ + irr	785	grey dep, hex 100–250 μm(l) × 5 μm (w) ⫰ + 10 μm ◆	64		
83	1500 (**1a**) [16.3]	{**I**} 1500 [10.3]	~ 65% fill @ − 33 °C	500 °C, 6d	yel pdr, 90% cub 200 nm–1 μm ◆	400	gr dep, hex 25–150 μm ⫰	109	gr dep, hex 100–300 μm ⫰	4

▲ = tetrahedra, △ = triangular prisms, ◬ = etched/bundled triangular prism, irr = irregular, ⊙ = particles, ✶ = hex star-shaped rods, ⅄ = 3-sided star cluster, ⫰ = individual hex needles, ‖ = bundles of hex needles, ⋗ = wedges, ⩓ = nested cones or plates, pwdr = powder, dep = deposit, ndl = needle, ◇ = various polyhedral prisms, hex = hexagonal, or = orange, cub = cubic, yel = yellow, grn = green, brn = brown, wh = white, dk = dark.

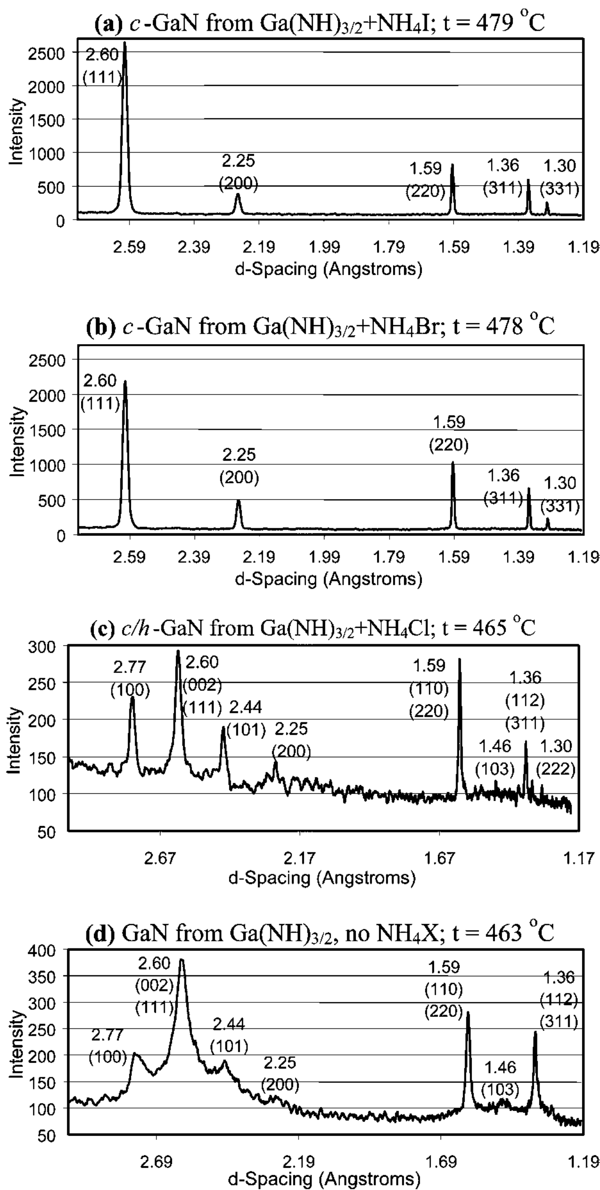

Fig. 1. Powder XRD spectra from selected sealed quartz tube experiments. Ammonothermal conversion of gallium imide, $\{Ga(NH)_{3/2}\}_n$, with (a) NH_4I (exp #72); (b) NH_4Br (exp #74); (c) NH_4Cl (exp #77); and (d) no mineralizer (exp #78).

The use of NH_4Br as the mineralizer seems to effect the formation of both cubic and hexagonal forms with the hexagonal form remaining the bottom of the tube and the cubic form actually transporting and depositing on the walls of the tube. In some cases, the deposited material contained both cubic and hexagonal phases (#64). In most experiments involving **1** and NH_4Br the GaN formed was greenish gray to dark green in color (Fig. 1c). An interesting note in all experiments involving **1** and NH_4Br is that an NH_3-insoluble white chunky material, presumably some intermediate gallium-bromide species, formed at or near the top of the tube and, in some cases, may have prevented deposition of GaN on the walls of the tube because of mechanical blockage. This white material was soluble in aqueous solvents and therefore removed during the washings associated with product recovery.

The use of NH_4Cl as a mineralizer for the conversion of **1** resulted chiefly in the formation of nanocrystalline material or hexagonal GaN. Powder XRD data showed that the GaN in the transported/deposited material was hexagonal phase. This material was gray with a light green tinge. The powder remaining in the bottom of the tube was amorphous showing no peaks in the powder x-ray diffraction pattern and, in some cases, was soluble in water or acid. Also, formation of an NH_3-insoluble white chunky material, similar to that in the NH_4Br case, was observed. This white material was soluble in aqueous solvents and removed during product recovery. Presumably this gallium halide species forms in all cases but is not observed when the halide is iodide because of it's increased solubility in liquid ammonia. In terms of solubility in liquid ammonia, $GaCl_3 < GaBr_3 \ll GaI_3$. The presence of low solubility Ga bromide and chloride species has been observed in previous ammonothermal reactions, and may account for some problems with reproducibility that occur with ammonothermal reactions in narrow tubes in which Ga metal is used as the feedstock [19].

The use of $NH_4X + LiX$ ($X = I$, Br) as a mineralizer system gave less than promising results. The addition of lithium halide seemed to interfere with not only GaN transport and deposition but, in the bromide case, actually prevented complete conversions of **1** to GaN. For these reasons experimentation using lithium halide additives with **1** was stopped. This is in marked contrast to results from the ammonothermal recrystallization of *h*-GaN to *c*-GaN, where LiX addition is highly beneficial for the *crystal growth process*, especially when $X = Cl$ [18]. An explanation may be that LiX addition affects the individual steps in the ammonothermal synthesis/crystal growth of GaN differently. Conversion of **1** to GaN and its transport may be completely independent processes. When starting from *h*-GaN feedstock, LiX addition dramatically increases the rate at which the

feedstock is dissolved in the hot zone and transported to the cool zone, and the amount of *c*-GaN in the deposit. When starting from Ga metal, LiX addition increases the fraction of *h*-GaN in the material formed from reaction of Ga with NH_3 in the hot zone, but also enhances the deposition of *c*-GaN in the cool zone. If LiX addition inhibits the conversion of **1** to GaN by disrupting the dissolution of **1** in the first place, the data are rather consistent. It is entirely conceivable that the Li^+ ion, being only slightly larger than Ga^{3+}, could bind to surface sites and affect the reactivity of the imide. Thus, the results from exp #73, in which the product at the tube bottom was 50% *h*-GaN while the deposit was *c*-GaN, are completely consistent with prior work. Complete results and analysis of LiX addition to the Ga/NH_4X ammonothermal reaction and other systems will be published at a later date [19].

With the use of **1** and NH_4I we are now able to prepare phase pure *c*-GaN powders. For this procedure to be useful, however, it must be scaled such that large crystals capable of being used for seed crystals in other crystal growth applications, or as substrates themselves can be produced. Sealed quartz tube experiments reveal that the most efficient conversion of **1** to *c*-GaN followed by transport and deposition is achieved when the masses of **1** and NH_4I are approximately equivalent. This is consistent with the reported result that phase-pure *c*-GaN is produced at 300 °C from ammonothermal reaction of Ga and NH_4I in a Pt lined vessel when at least 50 mol% of NH_4I is used [20]. It is interesting to note, however, the dependence of the crystallite size, morphology, and transport efficiency on not only the identity of the mineralizer, but also the quantity.

Figures 2a and 2b are SEM photographs of *c*-GaN grown in the cool zone from the ammonothermal transport of **1** with NH_4I. Clearly observable in Figs. 2a and 2b is the distinct triangular prismatic morphology common to the cubic form of GaN [9, 15, 18]. These crystals show extensive etching and pitting, as do the ammonothermally deposited *c*-GaN crystals in most of the experiments in Table I. Additionally, some of the open structure observable in Fig. 2a could result from a large number of crystallites growing in a bundle, almost in crystallographic registry with each other. Figure 2c shows the SEM of *c*-GaN grown from **1** with NH_4**Br** for comparison, which shows a similar kind of overgrowth of triangular plates to that evident in Fig. 2b.

Two of the experiments utilizing NH_4I as the mineralizer produced unique structures that are worth mentioning. Star-like clusters of *c*-GaN deposited in the coolest zone in exp #68 are shown in Fig. 2d. Numerous submicron polyhedra of various shapes are also present in this sample, e.g., the 600 nm cube attached to the star. The two step heating program (297, 530 °C) in #69 produced yet another unique morphology (Fig. 2e)

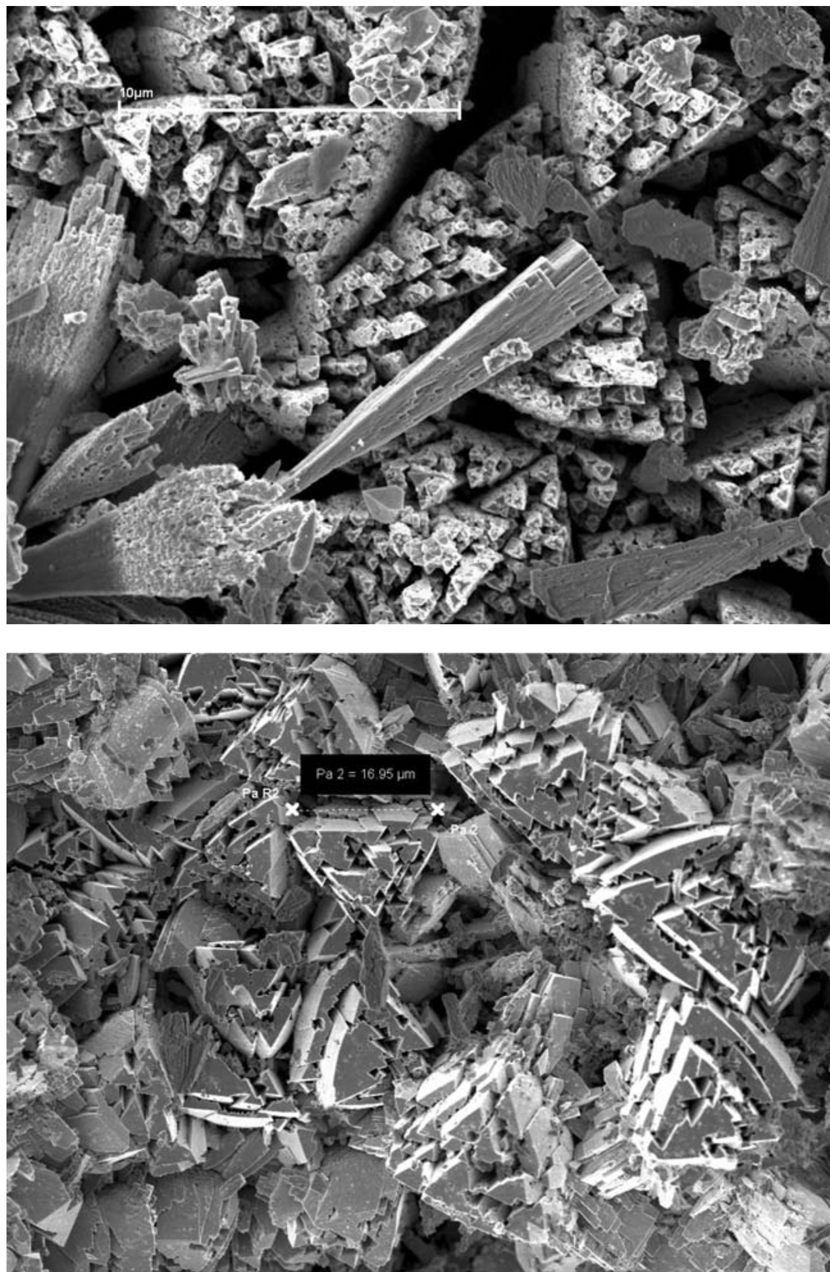

Fig. 2. (a) SEM image of *c*-GaN deposit grown in exp #72. (b) SEM image of *c*-GaN deposited in exp #76.

Fig. 2. (c) SEM image of *c*-GaN deposited in exp #74. (d) SEM image of star pattern of *c*-GaN crystals deposited in exp #68.

Fig. 2. (e) SEM Image of unique structure formed in lower (hotter) deposit of exp #69. (f) SEM image of *c*-GaN prepared in exp #71.

Fig. 2. (g) SEM image of the powder from the hot zone of exp #70. (h) SEM photo of product at tube bottom in exp #77.

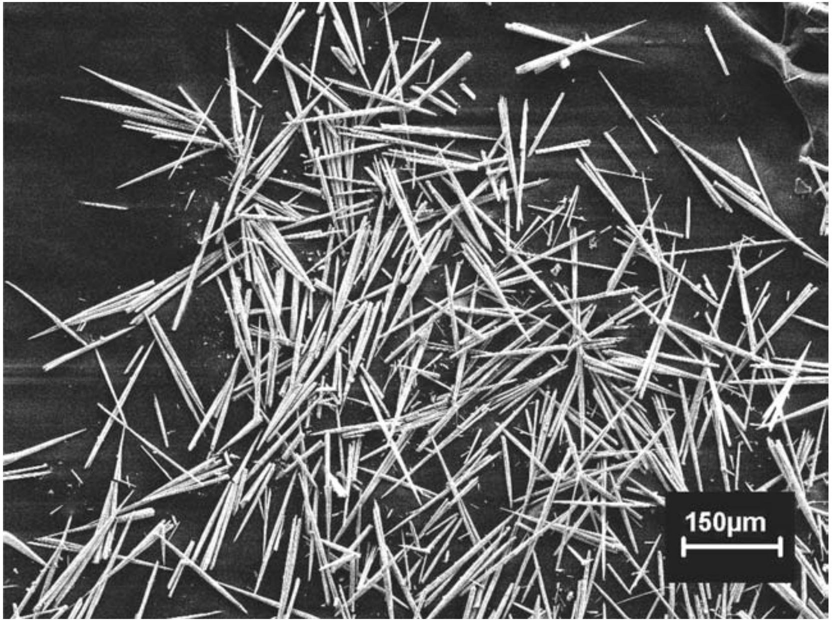

Fig. 2. (i) SEM image of needles deposited on sealing disc in exp #83.

in the warmest of the two deposition zones. The structure appears as a hexagonal star-shaped rod growing into nested cones or plates. Individually, both of these structures have been observed in ammonothermally deposited GaN [18], but never in combination.

In contrast, Fig. 2f is the SEM photograph of powder isolated from the bottom of exp #71 which contains regular un-etched tetrahedra of 1 μm or less in size in addition to heavily etched and pitted triangular prisms/wedges. The latter may have fallen down from the deposits in the upper portion of the tube. This result suggests that it should be possible to prepare tetrahedral nanoclusters of *c*-GaN if suitable conditions and capping agents can be found. Soluble nano-tetrahedra of Si have already been prepared [21]. However, it is evident that the size of the *c*-GaN tetrahedra are almost independent of the conversion temperature, as tetrahedra of about 1 μm size are produced from 305 to 510°C. Irregular nanoparticles are also present in many of these powders, particularly when **1** was converted at 510°C (exp #63). A curious formation was isolated from the bottom of exp #70 (Fig. 2g) which appears to be an agglomerate of tetrahedra, which may have been formed through a ripening/recrystallization process. Ripening apparently occurred in the powder produced with NH_4Br at 509°C as it consisted of mostly 1 μm hexagonal particles,

while those produced at a lower temperature (478 °C) were irregular nanoparticles. Both tetrahedra and 200 nm hexagonal prisms are clearly visible in the powder produced from the reaction with NH_4I/LiI mineralizer (exp #73). The powders produced from conversion of **1** with NH_4Cl at 465 and 511 °C (exps #65 and 77) consisted of mostly irregular (< 50 nm) nanoparticles (Fig. 2h). Ammonolysis of **1** in the absence of mineralizer (exp #78) produced material composed of irregular particles < 25 nm in diameter.

The use of quartz tubes with water overpressure limits the time, temperature, and most importantly the scale of these experiments. Not only is aqueous corrosion of quartz a limiting factor, but large diameter quartz tubes are incapable of the handling large pressure differentials unless the tubes are made impractically thick. We have found that Pt and Mo are fully resistant to corrosion by acidic ammonia, but only Pt lined vessels are commercially available. Several preliminary experiments were done to convert **1** to GaN in a Pt lined vessel using NH_4I mineralizer. Exp #81 demonstrated the potential for scale-up of the conversion of **1** to *c*-GaN. Notably, the *c*-GaN tetrahedra produced in this reaction were smaller than those made in the tubes and the low yield was probably due to losses during product recovery. At higher temperatures, starting with either **1** or **1a**, the product recovered from the bottom of the vessel was $\sim 90\%$ cubic phase, and the small amount of deposit at the top of the vessel was mostly needles of *h*-GaN. Some needles isolated from the surface of the Pt sealing disc in exp #83 are shown in Fig. 2i. The small amount of transport is probably due to excessive NH_3 fill of the autoclave, as excessive or insufficient fill shuts down chemical transport of *c*-GaN [15]. Interestingly, the siloxane contaminated material **1a** performed about the same as the pure imide, possibly because mechanical blockages could not occur in the 1.5″ diameter vessel in the way they did in narrow quartz tubes. Clearly, with additional work, this process can be optimized for the bulk synthesis of *c*-GaN powders from gallium imide.

ACKNOWLEDGEMENT

We thank the ONR for financial support.

REFERENCES

1. D. A. Neumayer and J. G. Ekerdt (1996). *Chem. Mater.* **8**, 9.
2. O. Ambacher (1998). *J. Phys. D Appl. Phys.* **31**, 2653.
3. B. Monemar (1999). *J. Mat. Sci. mater. Electr.* **10**, 227.
4. H. Yang *et al.* (1999). *Appl. Phys. Lett.* **74**, 2498.

5. S. Porowski (1998). *J. Cryst. Growth* **189/190**, 153.
6. H. Yamane *et al.* (1997). *Chem. Mater.* **9**, 413.
7. M. Aoki *et al.* (2000). *J. Cryst. Growth* **218**, 7.
8. H. Yamane, M. Shimada, and F. J. DiSalvo (2000). *Mater. Lett.* **42**, 66.
9. H. Yamane *et al.* (2000). *Jpn. J. Appl. Phys.* **39**, L146.
10. D. R. Ketchum and J. W. Kolis (2001). *J. Cryst. Growth* **222**, 431.
11. R. Dwilinski *et al.* (1998). *Diamond Rel. Mater.* **7**, 1348.
12. R. Dwilinski *et al.* (1996). *Acta Phys. Polonica A* **90**, 763.
13. M. Callahan *et al.* (1999). *MRS Internet J. Nitride Semicond. Res.* **4**, 1.
14. M. Suscavage *et al.* (2001). *Phys. Status. Solidi.* **188**, 477.
15. A. P. Purdy (1999). *Chem. Mater.* **11**, 1648-1651.
16. J. A. Jegier *et al.* (2000). *Chem. Mater. 12*, **1003.**
17. J. F. Janik and R. L. Wells (1996). *Chem. Mater.* **8**, 2708.
18. A. P. Purdy, R. J. Jouet, and C. F. George, (2002). *Crystal Growth and Design* **2**, 141.
19. A. P Purdy *et al.*, in preparation.
20. W. Y. Wang *et al.* (2001). *Mat. Res. Bull.* **36**, 2155.
21. R. K. Baldwin *et al.* (2002). *J. Am. Chem. Soc.* **124**, 1150.